JCTC Journal of Chemical Theory and Computation

Article

pubs.acs.org/JCTC

Multistate λ-Local-Elevation Umbrella-Sampling (MS-λ-LEUS): Method and Application to the Complexation of Cations by Crown Ethers

Noah S. Bieler, Jan P. Tschopp, and Philippe H. Hünenberger*

Laboratory of Physical Chemistry, ETH Zürich, CH−8093 Zürich, Zürich, Switzerland

Supporting Information

ABSTRACT: An extension of the λ-local-elevation umbrella-sampling (λ-LEUS) scheme [Bieler et al. *J. Chem. Theory Comput.* **2014**, *10*, 3006] is proposed to handle the multistate (MS) situation, i.e. the calculation of the relative free energies of multiple physical states based on a single simulation. The key element of the MS-λ-LEUS approach is to use a single coupling variable Λ controlling successive pairwise mutations between the states of interest in a cyclic fashion. The Λ variable is propagated dynamically as an extended-system variable, using a coordinate transformation with plateaus and a memory-based biasing potential as in λ-LEUS. Compared to other available MS schemes (one-step perturbation, enveloping distribution sampling and conventional λ-dynamics) the proposed method presents a number of important advantages, namely: (*i*) the physical states are visited explicitly and over finite time periods; (*ii*) the extent of unphysical space required to ensure transitions is kept minimal and, in particular, one-dimensional; (*iii*) the setup protocol solely requires the topologies of the physical states; and (*iv*) the method only requires limited modifications in a simulation code capable of handling two-state mutations. As an initial application, the absolute binding free energies of five alkali cations to three crown ethers in three different solvents are calculated. The results are found to reproduce qualitatively the main experimental trends and, in particular, the experimental selectivity of 18C6 for K^+ in water and methanol, which is interpreted in terms of opposing trends along the cation series between the solvation free energy of the cation and the direct electrostatic interactions within the complex.

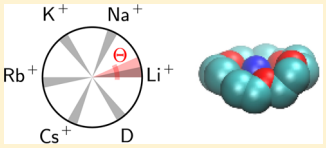

1. INTRODUCTION

The determination of binding free energies is central to the understanding of numerous (bio)chemical processes, including host−guest complexation chemistry,[1] metabolic pathway regulation,[2] enzyme catalysis,[3] or surface chemistry,[4] and it is also a key component of drug design.[5,6] Computational approaches, and in particular molecular dynamics (MD) simulations, offer nowadays a theoretical tool for the evaluation of binding free energies in solution based on elementary molecular physics.[7−10] Because the accuracy of these calculations is still limited,[11,12] they cannot at present substitute for a quantitative experimental determination. However, even in cases where the agreement with experiment is only qualitative, they can provide a wealth of additional information regarding the mechanisms at the molecular level, the driving forces in interplay, and the properties of intermediate species. In the absence of experimental data, their qualitative predictions can also be used to suggest (at limited costs) directions where additional (more expensive) experimental investigations will present the highest likelihood of success.

The main sources of errors in theoretical free-energy calculations are related to the approximate force-field representation of the systems and the finite sampling time of the simulations.[7−12]Besides the permanent effort of the community to construct more accurate force fields,[13−16] the design of efficient calculation methodologies addresses the problem of obtaining the most accurate possible results given a finite amount of sampling (computer) time.[11,12,17−21]

Because many binding processes occur on a long time scale relative to that currently accessible by MD, the monitoring of multiple binding-unbinding events in a simple MD simulation is seldom a feasible approach.[22] Even with the application of a conformational biasing, direct host−guest association remains challenging to sample.[23−25] For this reason, most of the *absolute* binding free-energy calculations to date have relied on a *double-decoupling* scheme.[26,27] In this approach, the guest is alchemically mutated to a molecular skeleton (same intramolecular interactions. But no interactions with the environment) either bound to the host or free in solution. A thermodynamic cycle is then invoked to relate the difference between the two values to the host−guest binding free energy in solution, taking into account that the host−skeleton binding free energy is zero.

If one wishes to calculate the *relative* binding free energies of N different guests to the same host, a situation common in drug design, a reference guest or state R must be selected. A series of N (or $N-1$ if R is one of the guests) *double-mutations* are then performed that convert R into each one of the (other) guests, either bound to the host or free in solution. These mutations typically involve much smaller perturbations compared to the full decoupling of the N guests and are thus typically easier to converge. The efficiency can be further enhanced by selecting an unphysical reference state R designed for optimal conformational-ensemble overlap with the N guests.[28−32] If desired, the

Received: February 7, 2015

DOI: 10.1021/acs.jctc.5b00118
J. Chem. Theory Comput. XXXX, XXX, XXX−XXX

absolute binding free energies of the N guests can be recovered by applying the double-decoupling approach either to only one of them or to R.

The obvious next methodological step is to design a procedure for calculating the *entire set* of relative binding free energies for N guests based on a *single pair* of simulations, one within the host and one free in solution. This approach will be referred to here as a *multistate* (MS) free-energy calculation, and the two simulations involved will be referred to as the *reference* simulations. In addition to a potential gain in efficiency, a working approach of this kind would represent a great simplification in the calculation protocol and can be considered as a holy grail in the area of drug design. Among the schemes proposed toward this endeavor, one may mention the MS applications of one-step perturbation[28−30,33,34] (OSP), enveloping distribution sampling[35] (EDS), and λ-dynamics[36−41] (λD).

The main challenges to be addressed by these types of approaches are: (A) to generate a reference simulation that samples configurations overlapping with those relevant for all of the N physical states;[28−30,35−41] (B) to reduce the sampling of irrelevant configurations to a strict minimum, ideally to the smallest possible number of configurations required for ensuring frequent transitions between the relevant regions;[18,19,42] (C) to provide a reliable estimator for the accuracy of the N calculated free-energy differences;[9,10] and (D) to be compatible with a simple (if possible, entirely automatic) setup and preoptimization procedure prior to the generation of the reference simulations. These challenges are met to different extents by the methods available to date, the most crucial shortcomings being (arguably) points A, C, and D for OSP when using a soft-site reference state,[33,34,43−45] point B for EDS, and points B and C for λD in the implementation of refs 36−41. Note that in all cases, early work in the field[28,30,46] has made clear that purely extrapolative schemes do not work well. Any reliable MS approach requires *a priori* knowledge of the N physical states in order to design an appropriate reference simulation.

The present study focuses on the MS application of the λD method. Its aim is to show that our recently proposed λ-local-elevation umbrella-sampling (λ-LEUS) method,[47] which combines the original λD scheme[36] with the LEUS biasing approach[48] (the latter being a combination of the LE searching[49] and US sampling[50] methods), can easily be extended into a very effective (in terms of properties A−D above) MS-λ-LEUS scheme.

When considering a pair of states A and B with Hamiltonians $\mathcal{H}_A$ and $\mathcal{H}_B$ (e.g., molecular topologies corresponding to two different guests), an alchemical mutation is controlled by a hybrid Hamiltonian $\tilde{\mathcal{H}}$ depending on a coupling parameter λ, such that $\tilde{\mathcal{H}} = \mathcal{H}_A$ for $\lambda = 0$ and $\tilde{\mathcal{H}} = \mathcal{H}_B$ for $\lambda = 1$. Many different methods[29,36,51−57] can then be applied to evaluate the potential of mean force $G(\lambda)$ based on an MD simulation (or a set thereof), and thus the free-energy difference $\Delta G_{AB} = G(1) - G(0)$. In the λD scheme,[36] λ is promoted from the role of parameter to that of dynamical variable, i.e. it is assigned a mass parameter, a dynamical momentum variable, a kinetic energy contribution, and an equation of motion. We recently introduced the λ-LEUS scheme[47] as an attempt to remedy a number of shortcomings of the original λD approach.[36] In particular, by distinguishing the Hamiltonian coupling variable λ from a corresponding dynamical variable θ and introducing a periodic coordinate transformation[40,41,58−62] $\lambda(\theta)$ with plateaus,[47] it was possible to enforce the finite sampling of the physical states A and B. In addition, quasi-homogeneous sampling along θ as well as a high number of transitions could be achieved using the LEUS memory-based biasing scheme,[48] possibly starting from an initial biasing potential obtained via slow-growth memory guessing[63] (SGMG). Finally, reasonable choices were suggested for the mass parameter and for the thermostatting scheme of the alchemical variable.[47,64]

Several studies[37−41] have proposed an extension of the original λD approach[36] to the MS situation, i.e. considering a collection of several physical states. The strategy employed was to generalize the scalar coupling variable λ into an N-dimensional vector $\boldsymbol{\lambda}$ defining a complete linear combination of all the states, such that a vector corresponds to a state n when $\lambda_n = 1$ and all the other components are set to zero. The vector components then evolved individually with the constraint that their sum remains equal to one at any time. In addition to the shortcomings[47] specific to the two-states λD approach,[36] this setup has the additional drawback in the MS context that it opens up a very large extent of irrelevant space to sampling (point B above), namely a $\boldsymbol{\lambda}$-space of $N-1$ dimensions (N variables, one constraint) in which only N infinitesimal points are actually physically relevant.

Here, we suggest a straightforward extension of the λ-LEUS scheme[47] to the MS situation that would not be affected by this problem. In the proposed strategy, the scalar coupling variable λ is generalized into a periodic variable Λ (with the reference period $[0;N[$) controlling the values of the individual λ_n (within the range $[0;1]$) in a piecewise fashion. This is done by concatenating into Λ successive unit ranges that convert one state to the next in the sequence, without any contribution from the other states, and terminating by a range converting the last state back into the first one. After application of a corresponding periodic coordinate transformation $\Lambda(\Theta)$ including a plateau for each state, the irrelevant space should be considerably reduced, as the space to be sampled is given by a one-dimensional Θ-space with N finite segments relevant for the physical states.

After describing the proposed MS-λ-LEUS scheme in detail, an initial application of the method in the context of host−guest chemistry is reported, namely the calculation of the absolute binding free energies of five alkali cations to three crown ethers in three different solvents. In their most basic form, crown ethers are cyclic oligomers of the ethyleneoxy fragment $-CH_2-CH_2-O-$. They were originally developed by Pedersen[65] in 1967 and have found a wide range of applications, in particular for cation solvation in organic solvents[66−69] or cation extraction from polar solvents.[66,70,71] The calculation of the binding free energies of various cations to these compounds has already been the scope of a number of theoretical studies.[72−76]

The three crown ethers considered here are illustrated in Figure 1. These are labeled 12C4, 15C5, and 18C6, where the two numbers in the abbreviation[77] refer to the total number of nonhydrogen atoms and the total number of oxygen atoms, respectively. For each of the three hosts and considering the solvents water (H_2O), methanol (CH_3OH), and dimethyl sulfoxide (DMSO), the absolute binding free energies of the five alkali cations (Li^+, Na^+, K^+, Rb^+, and Cs^+) are calculated using the proposed MS-λ-LEUS approach. More precisely, for each host and solvent, two reference simulations (harmonically restrained within the host or free in solution) are required

DOI: 10.1021/acs.jctc.5b00118
J. Chem. Theory Comput. XXXX, XXX, XXX−XXX

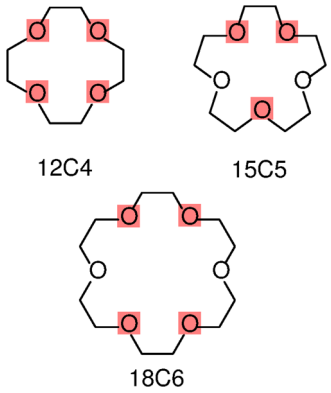

Figure 1. Crown ethers considered in this study. The three crown ethers (hosts) are 12C4, 15C5, and 18C6. The oxygen atoms used for the restraining of the ion (guest) within the complex, see eq 8, are highlighted in red.

where six states can dynamically interconvert along the periodic sequence $Li^+ \rightarrow Na^+ \rightarrow K^+ \rightarrow Rb^+ \rightarrow Cs^+ \rightarrow D \rightarrow Li^+$, where D is a dummy atom (mass point exempt of nonbonded interactions). After application of a thermodynamic cycle and correcting for the influence of the harmonic restraints in the complex and for the standard-state definitions,[27,78,79] the results are compared to the corresponding experimental data[69−71,77] whenever available.

2. THEORY

The λ-LEUS method as applied to a two-state problem[47] relies on a Hamiltonian of the form

$$\mathcal{H}(\theta) = \tilde{\mathcal{H}}(\lambda(\theta)) + \frac{p_\theta^2}{2m_\theta} + \mathcal{B}(\theta) \tag{1}$$

leading to the equations of motion

$$\dot{\theta} = \frac{p_\theta}{m_\theta} \quad \text{and} \quad \dot{p}_\theta = -\frac{\partial \mathcal{H}}{\partial \theta} \tag{2}$$

for the dynamical variable θ and its conjugate momentum p_θ. Here, m_θ is the mass parameter (with units of u nm^2 where u = g mol^{-1}), $\tilde{\mathcal{H}}$ is the hybrid Hamiltonian, λ is the associated coupling variable defined in such a way that $\tilde{\mathcal{H}}(0) = \mathcal{H}_A$ and $\tilde{\mathcal{H}}(1) = \mathcal{H}_B$, $\lambda(\theta)$ is a coordinate transformation, and $\mathcal{B}(\theta)$ is a biasing potential. For simplicity, the dependence of the Hamiltonians on the Cartesian coordinates $\boldsymbol{r}$ and momenta $\boldsymbol{p}$ of the physical particles is not indicated explicitly.

The coordinate transformation $\lambda(\theta)$ is a periodic flat-tip zigzag curve, alternating segments of slope $\pm W^{-1}$ with plateaus of width w at $\lambda = 0$ or 1

$$\lambda(\theta) = \begin{cases} 0 & \text{if } 0 \le \theta \le w \\ \dfrac{\theta - w}{W} & \text{if } w < \theta < \dfrac{P}{2} \\ 1 & \text{if } \dfrac{P}{2} \le \theta \le \dfrac{P}{2} + w \\ \dfrac{P - \theta}{W} & \text{if } \dfrac{P}{2} + w < \theta < P \end{cases} \tag{3}$$

where $P = 2\,(W + w)$ is the period onto which θ is refolded. The flat tips (plateaus) ensure the finite sampling of the λ values corresponding to the physical end states.

The biasing potential is constructed adaptively (LE build-up phase) and then frozen (US sampling phase), following the principles of the LEUS approach,[47,48] starting from an initial memory that can either be set to zero[47] or initialized by means of an inexpensive preliminary SGMG calculation.[63] This biasing procedure ensures a quasi-homogeneous sampling along θ as well as a high number of transitions between the end states during the US phase. Finally, the free-energy difference between the two states is calculated by reweighting, as

$$\Delta G_{AB} = -\beta^{-1} \ln \frac{\langle \delta[\lambda(\theta) - 1] \exp[+\beta \mathcal{B}(\theta)] \rangle_{\mathrm{US}}}{\langle \delta[\lambda(\theta) - 0] \exp[+\beta \mathcal{B}(\theta)] \rangle_{\mathrm{US}}} \tag{4}$$

where δ is the Dirac function, $\langle \ldots \rangle_{\mathrm{US}}$ denotes a biased ensemble average over the US phase, and $\beta = (k_{\mathrm{B}}T)^{-1}$, k_{B} being the Boltzmann constant and T the absolute temperature.

To extend the above scheme to a MS situation involving N states $n = 0, \ldots, N-1$, the two-state coupling variable λ is generalized into a periodic variable Λ (with the reference period $[0;N[$) controlling the values of N individual λ_n parameters (within the range $[0;1]$) in a piecewise and circular fashion. For integer values $\Lambda = n$ with $n = 0, \ldots, N-1$, the coupled Hamiltonian corresponds to that of the physical state n. The value $\Lambda = N$ is again associated with the Hamiltonian of the first state, i.e. the same as for $\Lambda = 0$. For a noninteger value of Λ comprised between integers n and $n + 1$ with $n = 0, \ldots, N-2$, the coupled Hamiltonian is a hybrid between those of the states n and $n + 1$, the corresponding coupling parameter λ_n being equal to $\Lambda - n$. Finally, for a value of Λ comprised between $N-1$ and N, the coupling occurs between state $N-1$ and state 0, while the corresponding coupling parameter λ_{N-1} is equal to $\Lambda - (N-1)$. In summary, as Λ is progressively increased from 0 to N, the coupled Hamiltonian cycles in a continuous fashion through the N different states, starting from and returning to state 0. Note that a state sequence along the cycle must be specified and that this choice may have some influence on the convergence properties of the method in practice but not its results in the limit of infinite sampling.

There are two main advantages of using a so-defined Λ coupling variable instead of a $\boldsymbol{\lambda}$ vector as in refs 37−41: (*i*) the space associated with the alchemical variable remains one-dimensional instead of becoming $(N-1)$-dimensional (see the Introduction); and (*ii*) the state coupling only involves pairs of states, although the coupled pairs change for successive unit intervals along Λ, which implies only limited modifications in an MD simulation code that is able to handle two-state mutations.

The coordinate transformation $\lambda(\theta)$ of eq 3 must be generalized accordingly to a corresponding transformation $\Lambda(\Theta)$ given by

$$\Lambda(\Theta) = \begin{cases} \nu & \text{if } \dfrac{\Theta - (\nu + 1)w}{W} < \nu \\ \dfrac{\Theta - (\nu + 1)w}{W} & \text{otherwise} \end{cases} \tag{5}$$

with $\nu = \left\lfloor \frac{\Theta}{W + w} \right\rfloor$ where $\lfloor \cdots \rfloor$ denotes the floor-integer function. The period of Θ is $N(W+w)$ and the generated Λ-range is restricted to the reference period $[0;N[$, i.e. excluding

DOI: 10.1021/acs.jctc.5b00118
J. Chem. Theory Comput. XXXX, XXX, XXX−XXX

N. It is easily seen that the special case with $N = 2$ (two states A and B) is equivalent to eq 3, when interpreting λ_0 as λ and λ_1 as $1 - \lambda$, λ being the coupling parameter of the $A \rightarrow B$ mutation. The function defined in eq 5 is illustrated graphically in Figure 2 for the six-state situation ($N = 6$) considered in the present application to crown ethers.

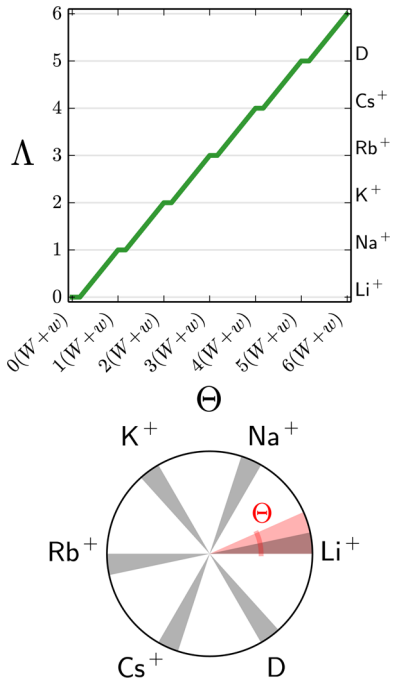

Figure 2. Coordinate transformation used in the MS-λ-LEUS scheme. The graph (top) illustrates the coordinate transformation $\Lambda(\Theta)$ of eq 5 for the six-state situation ($N = 6$) considered in the present application to crown ethers. The states are in sequence Li^+, Na^+, K^+, Rb^+, and Cs^+, followed by a dummy atom D. The dial (bottom) illustrates how the six states are visited in a cyclic fashion (counterclockwise in the illustration) over a period $N(W+w)$ of Θ, including constant-Λ sectors of width w (gray) ensuring finite sampling of the physical states.

The corresponding forms for the Hamiltonian and equations of motion are given by eqs 1 and 2 with θ and λ substituted by Θ and Λ, respectively. Finally, the potential of mean force (PMF) along Θ is calculated as

$$G(\Theta') = -\beta^{-1}\ln\langle\delta[\Theta - \Theta'] \exp[+\beta\mathcal{B}(\Theta)]\rangle_{US} + \boldsymbol{C} \quad (6)$$

and the free energy of a state n is obtained in analogy to eq 4 as

$$G_n = -\beta^{-1}\ln\langle\delta[\Lambda(\Theta) - n] \exp[+\beta\mathcal{B}(\Theta)]\rangle_{US} + \boldsymbol{C}' \quad (7)$$

where $\boldsymbol{C}$ and $\boldsymbol{C}'$ are arbitrary constants.

3. COMPUTATIONAL DETAILS

3.1. Simulated Systems. Free-energy calculations using the MS-λ-LEUS method were carried out to evaluate the absolute binding free-energies of five possible guests to three different hosts in three different solvents at 300 K and 1 bar. The guests considered are the five alkali cations (Li^+, Na^+, K^+, Rb^+, and Cs^+). The calculations also required the consideration of the dummy atom D, a mass point exempt of nonbonded interactions, which is referred to below as a sixth guest. The hosts considered are the three crown ethers shown in Figure 1, namely 12C4, 15C5, and 18C6. The calculations also relied on simulations of the guests free in solution. The four situations (three hosts plus free) are referred to below as different environments. The solvents considered are water (H_2O), dimethyl sulfoxide (DMSO), and methanol (CH_3OH). For a given solvent and environment, the calculation of the relative free energies of the states corresponding to the six guests relied on a single MS-λ-LEUS simulation, resulting in a total of 12 simulations for the entire study. In each of these calculations, the arbitrary constants in eqs 6 and 7 were defined by setting the free energy of the dummy-guest state to zero. For a specific solvent and considering an ion I, the resulting relative free energy of eq 7 is noted ΔG_I^{host} for the ion within a given host and ΔG_I^{free} for the free ion in solution. Comparing ΔG_I^{host} and ΔG_I^{free}, the standard absolute binding free-energy ΔG_I° can be calculated (see further below).

The simulations were carried out under periodic boundary conditions based on cubic computational boxes. To minimize the influence of finite-size effects[80,81] on the results, the number of solvent molecules was selected individually in the 12 MS-λ-LEUS simulations, so as to enforce equal average box-edge lengths $L = 3.54$ nm in all cases. To further assess the magnitude of these effects, the calculations involving the solvents H_2O and CH_3OH were also repeated with $L = 3.2$ or 3.8 nm, requiring an additional set of 16 simulations. The number of solvent molecules involved in the different simulations are listed in Table 1. Only the results pertaining to $L = 3.54$ nm are reported in the tables and figures of the main article. Corresponding tables and figures including the results for the two alternative box sizes can be found in the Supporting Information.

3.2. Binding Restraints. In the MS-λ-LEUS simulations, the guest cycles between six different states, including the dummy state as well as various unphysical (soft-core) intermediate states. For this reason, the simulations involving

Table 1. Number of Solvent Molecules in the Different MS-λ-LEUS Simulations[a]

	solvent						
	$L = 3.54$ nm			$L = 3.2$ nm		$L = 3.8$ nm	
environment	H_2O	DMSO	CH_3OH	H_2O	CH_3OH	H_2O	CH_3OH
12C4	4316	1522	1967	3194	1469	5351	2483
15C5	4310	1525	1970	3188	1472	5345	2486
18C6	4307	1524	1973	3185	1475	5342	2489
free	4331	1518	1964	3209	1466	5366	2480

[a]For the different solvents and environments, the number of solvent molecules included in the cubic computational box is reported. A series of 12 simulations was carried out within boxes of common average box-edge length $L = 3.54$ nm. For the solvents H_2O and CH_3OH, additional simulations were performed using a smaller and a larger box, the corresponding results being reported in the Supporting Information.

DOI: 10.1021/acs.jctc.5b00118
J. Chem. Theory Comput. XXXX, XXX, XXX−XXX

a crown-ether host included binding restraints to prevent the guest from diffusing away into solution. These restraints were applied in the form of a half-harmonic potential depending on the (formally, minimum-image) distance r_{cog} between the guest and the center of geometry of three (15C5) or four (12C4 and 18C6) oxygen atoms of the host (see Figure 1), namely

$$U_{res} = \begin{cases} \frac{1}{2}K_{res}(r_{cog} - r_{res})^2 & \text{if } r_{cog} > r_{res} \\ 0 & \text{otherwise} \end{cases} \quad (8)$$

where the force constant K_{res} was set to 2000 kJ mol^{-1} nm^{-2}, and the switching distance r_{res} was set to 0.22, 0.17, and 0.10 nm for 12C4, 15C5, and 18C6, respectively. These distances were inferred from r_{cog} distributions monitored in separate simulations of the three ethers with the largest Cs^+ ion (data not shown). They decrease with increasing size of the ether because the ion can come closer to the center of the host when its cavity size is larger. The free-energy results were corrected for the effect of these restraints (see below).

3.3. Binding-Restraint and Standard-State Corrections. In a given solvent, the standard absolute binding free energy ΔG_I° of a specific ion I to a specific crown ether was calculated according to the thermodynamic cycle depicted in Figure 3, corresponding to the double-decoupling method[26,27]

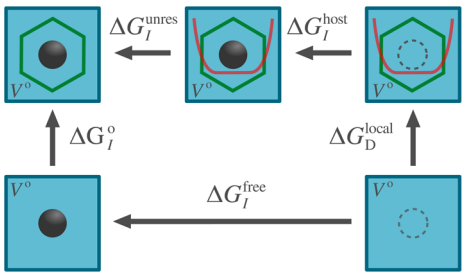

Figure 3. Thermodynamic cycle used for calculating the standard absolute binding free energy ΔG_I°. The thermodynamic cycle underlying eq 9 is shown for a specific mutation from a dummy atom (D, dashed circle) to an ion (I, full sphere), either free in solution (blue box), resulting in a free-energy change ΔG_I^{free}, or bound to a crown ether (green hexagon), resulting in a change ΔG_I^{host}. Due to the half-harmonic restraining (red curve) of the guest within the host, two correction terms are needed, namely ΔG_D^{local} in eq 10 and ΔG_I^{unres} in eq 12. The drawing and calculations refer to a standard-state reference volume V° (relevant only for ΔG_D^{local}).

with corrections for binding restraints and standard-state definition.[27,78,79] The resulting equation reads

$$\Delta G_I^\circ = \Delta G_I^{host} - \Delta G_I^{free} + \Delta G_D^{local} + \Delta G_I^{unres} \quad (9)$$

Note that the typically very small contribution of the pressure−volume term is neglected in this equation (last term in eq 13 of ref 27).

The correction term ΔG_D^{local} accounts for the localization of a dummy atom D close to the center of the crown-ether host under the action of the restraining potential. It is exclusively entropic in nature and given by

$$\Delta G_D^{local} = -\beta^{-1} \ln \frac{V_D^{res}}{V^\circ} \quad (10)$$

where V_D^{res} is the effective volume accessible to the dummy atom after localization, and V° is the accessible solution volume corresponding to the standard-state definition. The effective volume V_D^{res} is calculated analytically as

$$V_D^{res} = 4\pi \int_0^\infty e^{-\beta U_{res}} r_{cog}^2 dr_{cog} = 4\pi \frac{r_{res}^3}{3} + \left(\frac{2\pi}{\beta K_{res}}\right)^{3/2} \left(1 + 4\sqrt{\frac{\beta K_{res}}{2\pi}} r_{res} + \beta K_{res} r_{res}^2\right) \quad (11)$$

where it is assumed that the restraints are strong, so that the integration volume can be extended to the entire space for r_{cog}. The volume V° depends on the standard-state definition. For a molal reference concentration b° = 1 mol kg^{-1}, it is given by $V^\circ = (N_A \rho_{svt} b^\circ)^{-1}$, where ρ_{svt} is the pure-solvent density and N_A is the Avogadro number. For a molar reference concentration m° = 1 mol dm^{-3}, it is given by $V^\circ = (N_A m^\circ)^{-1}$ = 1.66 nm^3.

The correction term ΔG_I^{unres} accounts for the removal of the restraints in the complex of the ion I with the given crown ether. It can be estimated from the simulations using the OSP formula[29,54]

$$\Delta G_I^{unres} = -\beta^{-1} \ln \langle e^{+\beta U_{res}} \rangle_I \quad (12)$$

where $\langle \cdots \rangle_I$ denotes an ensemble average over the MS-λ-LEUS simulation restricted to the Θ values (plateau) associated with the presence of the ion I. The corresponding quantity calculated without this restriction and resolved as a function of Θ will be noted as $\Delta G^{unres}(\Theta)$.

In the special case where the ion I is the dummy atom D, eq 9, together with eq 10, the analytical evaluation of eq 12, and the observation that $\Delta G_D^{host} = \Delta G_D^{free} = 0$, leads to

$$\Delta G_D^{unres} = -\beta^{-1} \ln \frac{L^3}{V_D^{res}} \quad (13)$$

and

$$\Delta G_D^\circ = -\beta^{-1} \ln \frac{L^3}{V^\circ} \quad (14)$$

where L^3 is the volume of the computational box. Thus, as expected, the binding affinity of the dummy atom is zero, up to a standard-state correction term corresponding to localizing the dummy atom into the computational box. Note, however, that the value of ΔG_D^{unres} obtained from the simulations using eq 12 will never converge to the analytical value of eq 14 in practice, because the dummy atom would have to visit the entire box volume in spite of the binding restraints. However, this does not represent a problem since the term ΔG_D^{unres} is not required for the calculation of the absolute binding free energy ΔG_I° of any ion I using eq 9.

3.4. Simulation Parameters. All simulations were carried out using a modified version of the GROMOS MD++ program[82−84] implementing the MS-λ-LEUS algorithm. The parameters for the crown ethers were generated based on the 53A6$_{OXY+D}$ force field,[85] a variant of the 53A6$_{OXY}$ parameter set[86] specifically optimized for the accurate representation of the vicinal diether function. The Lennard-Jones interaction parameters for the alkali ions were taken from Reif and Hünenberger,[87] set L therein, where they were optimized against hydration free energies (including corrections for finite-size effects and based on a standard absolute hydration free-energy estimate of −1100 kJ mol^{-1} for the proton). The dummy atom D was defined as a particle of mass 15 u exempt of charge and Lennard-Jones interactions. The models

DOI: 10.1021/acs.jctc.5b00118
J. Chem. Theory Comput. XXXX, XXX, XXX−XXX

considered for the different solvents were the simple point charges (SPC) model of Berendsen et al.[88] for H_2O, the model of Geerke et al.[89] for DMSO, and the model of Walser et al.[90] for CH_3OH.

The equations of motion were integrated using the leapfrog algorithm[91] with a time step of 2 fs. All bond lengths as well as the water hydrogen−hydrogen distances were constrained by application of the SHAKE procedure[92] with a relative geometric tolerance of 10^{-4}. The temperature of the physical system was kept close to 300 K using weak coupling[93] to a single heat bath with a relaxation time of 0.1 ps. The pressure was maintained close to 1 bar using weak coupling[93] of the atomic coordinates and box dimensions (isotropic coordinate scaling, group-based virial) to a pressure bath with a relaxation time of 0.5 ps and compressibilities set to the experimental values[94,95] of 4.575, 8.718, and 12.98 in units of 10^{-4} kJ mol^{-1} nm^3 for H_2O, DMSO, and CH_3OH, respectively. The translational center of mass motion of the computational box was removed every 100 steps. The nonbonded interactions were calculated using a twin-range cutoff scheme[96] with short- and long-range cutoff distances set to 0.8 and 1.4 nm, respectively, and an update frequency of 5 timesteps for the short-range pairlist and intermediate-range interactions. The mean effect of the electrostatic interactions beyond the long-range cutoff distance was accounted for by means of a reaction-field correction[97,98] using a relative dielectric permittivity of 61 for the SPC water model[99] or the experimental values[94] of 47.2 and 33.0 for DMSO and CH_3OH, respectively.

For the MS-λ-LEUS simulations,[47] the cyclic state ordering was set to $Li^+ \rightarrow Na^+ \rightarrow K^+ \rightarrow Rb^+ \rightarrow Cs^+ \rightarrow D \rightarrow Li^+$. The successive mutations between pairs of states relied on a soft-core coupling scheme[100] with softening parameters $\alpha_{LJ} = 0.25$ and $\alpha_{CRF} = 0.25$ nm^2 for Lennard-Jones and electrostatic interactions, respectively. The inverse slope was set to $W = 1$, the plateau width to $w = 0.1$, the mass parameter[47,64] to $m_\theta = 75$ u nm^2, and the grid spacing for the cubic splines[47,101,102] basis functions to 0.1. The alchemical variable Θ was thermostated separately to 300 K using a Nosé−Hoover chain[103] of 10 thermostat variables, each with a relaxation time[47,64] of 0.1 ps. The biasing potential was initialized using the SGMG scheme,[63] based on slow-growth simulations of 132 ps duration. The LE build-up phase lasted for 30 ns and relied on an initial force-constant increment of 0.1 kJ mol^{-1} per time step along with a reduction factor[19,47] (scaling of the force-constant increment performed after completing each double-sweep of the entire Θ range) set to 0.6. The number of double-sweeps occurring in the LE phase was between 10 and 20 for the different simulations. Finally, the US sampling phase was carried out for 50 ns.

4. RESULTS

4.1. MS-λ-LEUS Scheme. As an illustrative example for the properties of the MS-λ-LEUS simulations, the time series of Θ, the corresponding probability distribution $p(\Theta)$, and the associated PMF $G(\Theta)$ are shown in Figure 4 for the US sampling phase of the simulations in water, either without crown ether or with 15C5. Corresponding graphs for the other simulations are qualitatively similar (data not shown). The Θ time series presents a high number of transitions between the physical states over 50 ns, visiting each state in about 150 (without crown ether) and 90 (with 15C5) distinct events on average over this time period. Compared to the pure-solvent environment, the transition rate is somewhat lower in the presence of the crown ether, probably due to the influence of slower conformational processes[73] within the host. However, in both cases, the probability distribution $p(\Theta)$ is essentially homogeneous over the entire range, except for some fringes at the edges of the plateaus and some deviations around the dummy state. The fringes are probably related to the sharp changes in the slope of the PMF at the plateau edges,[47] which may be inaccurately represented by the biasing potential, while the deviations around the dummy state are likely due to a slightly less good convergence of the biasing potential in this high-lying region of the PMF. As expected, the free energy $G(\Theta)$ at the plateaus corresponding to the cations is negative relative to that of the dummy atom, which does not interact with its environment. For the pure-solvent simulation, the hydration free energy becomes increasingly more negative from Cs^+ to Li^+, following the decrease in the ion size at constant charge. The same trend is observed in the presence of 15C5.

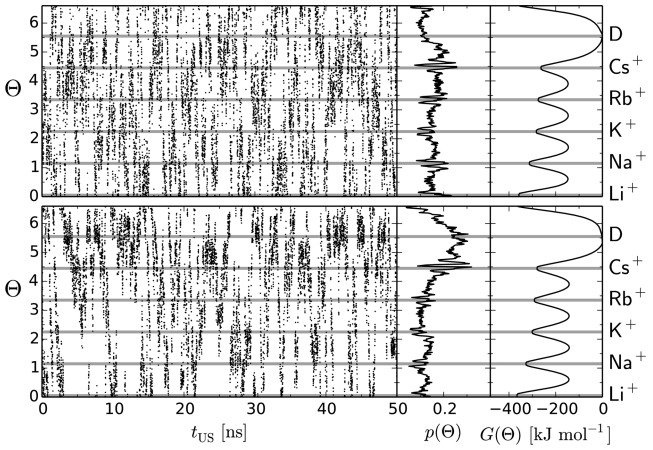

Figure 4. Properties of two illustrative MS-λ-LEUS simulations. The properties are shown for the US sampling phase of the simulations in water using the normal box (L = 3.54 nm), either in the absence of a host (top) or in the presence of 15C5. They are (from left to right) the time series of the alchemical variable Θ, the corresponding probability distribution $p(\Theta)$, and the associated PMF $G(\Theta)$ from eq 6, anchored to zero at the dummy state D. The plateau regions in Θ corresponding to the physical states are highlighted in gray.

4.2. Binding-Restraint and Standard-State Corrections. The binding restraints of eq 8 applied in the host−guest complexes must be selected in such a way that they prevent the guest from diffusing irreversibly into the solvent, without hindering the sampling of the relevant conformations of the complex. This implies in particular that the corresponding correction term ΔG_I^{unres} of eq 12 must remain of small magnitude. To assess whether the parameters selected for this restraining are appropriate, the quantity $\Delta G^{unres}(\Theta)$ is displayed as a function of Θ in Figure 5 for the simulations involving a crown-ether host (see also Figure S1 in the Supporting Information for the results with different box sizes). For the physical states, the correction term ΔG_I^{unres} is indeed of small magnitude (usually below 1.5 kJ mol^{-1}). However, it can become very significant at unphysical intermediate points.

The reason is that the state coupling involves soft-core interactions.[100] The softening of the nonbonded interactions at the unphysical intermediate states weakens the Lennard-Jones repulsion between the cation and the surrounding negatively charged atoms. These can approach at closer distances, resulting in more favorable electrostatic interactions; but since the crown-ether oxygen atoms are covalently linked to

DOI: 10.1021/acs.jctc.5b00118
J. Chem. Theory Comput. XXXX, XXX, XXX−XXX

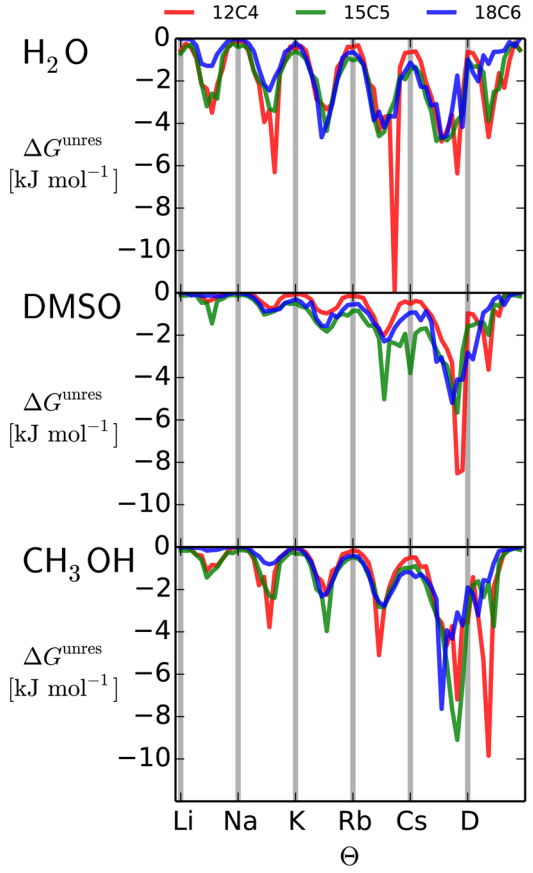

Figure 5. Correction term for releasing the binding restraints. The correction term $\Delta G^{\mathrm{unres}}(\Theta)$ of eq 12 with an unrestricted ensemble average and resolved as a function of Θ is displayed considering the simulations involving a crown-ether host in the normal box (L = 3.54 nm). The plateau regions in Θ corresponding to the physical states are highlighted in gray. The corresponding numerical values $\Delta G_I^{\mathrm{unres}}$ for the physical states are reported in Table 2. The results also including smaller and larger box sizes are shown in Figure S1 of the Supporting Information.

each other within the host, they are more restrained compared to the oxygen atoms of the solvent molecules. As a result, the ion−solvent interactions are artificially enhanced compared to the ion−host interactions, and the ion would escape into the solvent without the binding restraints. This explains why initial attempts to perform MS-λ-LEUS simulations in the absence of binding restraints (data not shown) nearly always resulted in the disruption of the complex, and why the magnitude of the correction term $\Delta G_I^{\mathrm{unres}}$ for these restraints is large at the unphysical intermediate states. Note that this issue is related to the form of the coupling scheme and not to the MS-λ-LEUS methodology, e.g. it would affect TI calculations as well.

The values of the corrections terms $\Delta G_{\mathrm{D}}^{\mathrm{local}}$ and $\Delta G_I^{\mathrm{unres}}$ of eqs 10 and 12, respectively, are reported in Table 2 for the different systems (see also Table S1 in the Supporting Information for the results with different box sizes). The correction term $\Delta G_{\mathrm{D}}^{\mathrm{local}}$ was calculated for a molar reference concentration m° = 1 mol dm^{-3}, resulting in V° = 1.66 nm^3. By comparison, the effective volume $V_{\mathrm{D}}^{\mathrm{res}}$ of eq 11, as determined by the parameters of the restraining potential, is much smaller, namely 0.08, 0.04, and 0.01 nm^3 for 12C4, 15C5, and 18C6, respectively. Since $V_{\mathrm{D}}^{\mathrm{res}} < V^\circ$, the correction $\Delta G_{\mathrm{D}}^{\mathrm{local}}$ must be positive, i.e. the volume restriction leads to an entropy decrease and thus to a free-energy increase. This term is significant (7.6−12.0 kJ mol^{-1}), and neglecting it in the calculation of the absolute binding free energies would induce a large error. Because the restraining energy U_{res} is everywhere positive or zero, the second correction term $\Delta G_I^{\mathrm{unres}}$ is always negative, i.e. the release of the restraint leads to an increase in the accessible volume and thus to a free-energy decrease. For the alkali cations, this term is at most 1.5 kJ mol^{-1} in magnitude, except for the complex of 15C5 with Cs$^+$ in DMSO, where it amounts to −3.8 kJ mol^{-1} (see the corresponding spike in the curve of Figure 5). As discussed earlier, for the dummy atom, the correction term $\Delta G_{\mathrm{D}}^{\mathrm{unres}}$ does not converge to its analytical value of eq 13 within the finite sampling time. This is not a problem considering that $\Delta G_{\mathrm{D}}^{\mathrm{unres}}$ is not needed in the calculation.

4.3. Relative Free Energies. The free energies ΔG_I of eq 7, given relative to the dummy state, are reported numerically in Table 3 and displayed graphically in Figure 6 for the different systems (see also Table S2 and Figure S2 in the Supporting Information for the results with different box sizes). For the free ions in solution, these relative free energies correspond to (nonstandard) solvation free energies and are expectedly large and negative. Their value increases monotonically with the ionic size from Li$^+$ to Cs$^+$, in agreement with the Born model[104] as well as with experimental and more advanced theoretical results.[105] According to the Born model, the magnitude of the solvation free energy should also increase with the solvent

Table 2. Correction Terms for the Calculation of the Standard Absolute Binding Free Energies[a]

			$\Delta G_I^{\mathrm{unres}}$ [kJ mol^{-1}]					
solvent	host	$\Delta G_{\mathrm{D}}^{\mathrm{local}}$ [kJ mol^{-1}]	Li$^+$	Na$^+$	K$^+$	Rb$^+$	Cs$^+$	D
H_2O	12C4	7.6	−0.6	−0.1	−0.5	−0.4	−0.6	(−0.6)
	15C5	9.1	−0.7	−0.4	−0.6	−1.0	−1.5	(−1.0)
	18C6	12.0	−0.0	−0.0	−0.2	−0.6	−1.1	(−1.0)
DMSO	12C4	7.6	−0.1	−0.0	−0.1	−0.1	−0.5	(−1.0)
	15C5	9.1	−0.1	−0.1	−0.5	−0.9	−3.8	(−1.6)
	18C6	12.0	−0.0	−0.0	−0.3	−0.5	−0.9	(−2.8)
CH_3OH	12C4	7.6	−0.0	−0.0	−0.1	−0.2	−0.5	(−3.6)
	15C5	9.1	−0.2	−0.1	−0.3	−0.5	−1.0	(−3.1)
	18C6	12.0	−0.0	−0.0	−0.0	−0.4	−1.2	(−1.9)

[a]The correction terms $\Delta G_{\mathrm{D}}^{\mathrm{local}}$ and $\Delta G_I^{\mathrm{unres}}$ are calculated using eqs 10 and 12, respectively, for the different solvents and hosts, considering the simulations in the normal box (L = 3.54 nm). The term $\Delta G_{\mathrm{D}}^{\mathrm{local}}$ assumes a one molar reference concentration (m° = 1 mol dm^{-3}). The term $\Delta G_I^{\mathrm{unres}}$ for the dummy atom (I = D) is given between parentheses, since it is neither converged nor necessary. The results also including smaller and larger box sizes are reported in Table S1 of the Supporting Information.

DOI: 10.1021/acs.jctc.5b00118
J. Chem. Theory Comput. XXXX, XXX, XXX−XXX

Table 3. Relative Free Energies Calculated from the MS-λ-LEUS Simulations[a]

		ΔG_I [kJ mol^{-1}]				
solvent		Li^+	Na^+	K^+	Rb^+	Cs^+
H_2O	12C4	−361.5	−321.4	−293.4	−284.6	−273.7
	15C5	−363.5	−325.0	−298.3	−289.1	−277.6
	18C6	−372.7	−336.3	−308.6	−299.0	−285.0
	free	−357.6	−312.6	−282.9	−274.5	−263.0
DMSO	12C4	−454.0	−407.2	−389.8	−380.8	−369.1
	15C5	−456.5	−410.5	−392.6	−383.7	−370.8
	18C6	−463.5	−426.3	−406.0	−396.5	−383.2
	Free	−446.4	−384.8	−374.2	−365.4	−353.1
CH_3OH	12C4	−412.1	−375.5	−347.6	−338.5	−326.5
	15C5	−414.4	−376.8	−350.6	−342.4	−329.8
	18C6	−427.4	−398.8	−372.6	−361.1	−345.4
	free	−395.7	−353.8	−324.2	−316.0	−304.5

[a]The free energies ΔG_I of eq 7, given relative to the dummy state, are reported for the different solvents and environments, considering the simulations in the normal box (L = 3.54 nm). This data is also illustrated graphically in Figure 6. The results also including smaller and larger box sizes are reported in Table S2 of the Supporting Information.

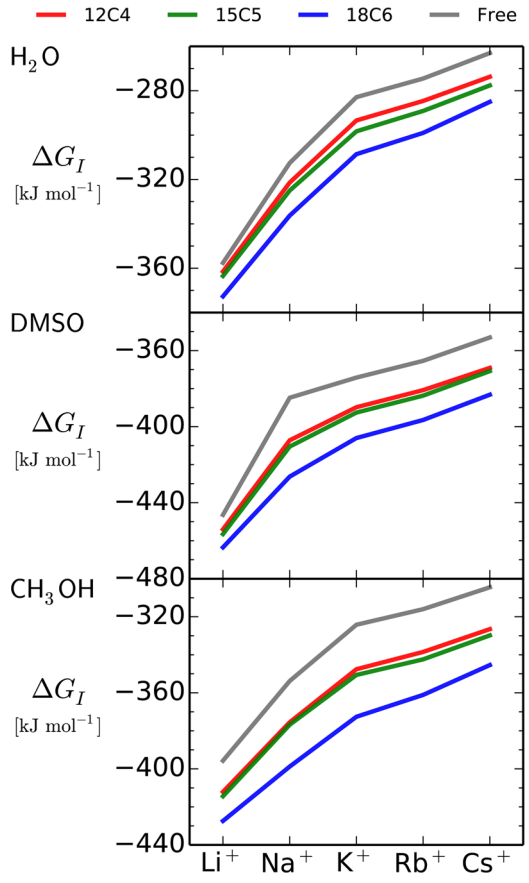

Figure 6. Relative free energies calculated from the MS-λ-LEUS simulations. The free energies ΔG_I of eq 7, given relative to the dummy state, are displayed for the different solvents and hosts, considering the simulations in the normal box (L = 3.54 nm). This data is also reported numerically in Table 3. The results including smaller and larger box sizes are shown in Figure S2 of the Supporting Information.

permittivity, i.e. in the order CH_3OH, DMSO, and H_2O. In practice, however, CH_3OH and to an even larger extent DMSO present more negative solvation free energies for the alkali cations compared to H_2O. In the case of DMSO, the inversion is in agreement with experiment[106] and related to asymmetric solvation effects,[107,108] namely the basity of DMSO (i.e., its propensity to solvate cations better than anions) is higher than that of water.[107] In the case of CH_3OH, the solvation free energies should be comparable to those in water,[106] and the apparent discrepancy may be in part related to the consideration of *raw* solvation free energies from the MD simulations, i.e. that are not corrected for possible cutoff, finite-size, potential-summation, and solvent-permittivity errors.[109,110] For the ions as guests within a crown-ether host, the relative free energy is more negative than the above solvation free energy by about 10−40 kJ mol^{-1} depending on the solvent, host, and cation. This dependence is at the origin of the trends observed in the calculated absolute binding free energies (see below).

4.4. Binding Free Energies. For the three solvents, three hosts, and five cations considered, the standard absolute binding free energies ΔG_I°, calculated from the MS-λ-LEUS simulations using eq 9, are reported numerically in Table 4 along with available experimental data.[69−71,77] The comparison is also performed graphically in Figure 7. All experimental values are assumed to pertain to a one molar reference concentration m° = 1 mol dm^{-3} as inferred from the quoted literature sources but not explicitly stated therein. However, if the experimental reference concentration was one molal instead, the corresponding error would be small for the solvents considered (at most 0.6 kJ mol^{-1}).

To minimize the influence of finite-size effects[80,81] on the results, the main calculations were performed using computational boxes of identical sizes L = 3.54 nm. However, the use of a common box size does not automatically guarantee a compensation of finite-size errors around the thermodynamic cycle, which also depends on the size and charge distribution of the host.[80] Thus, for the solvents H_2O and CH_3OH, the calculations were repeated considering a smaller (L = 3.2 nm) and a larger (L = 3.8 nm) box size. The corresponding results are provided in Table S3 and Figure S3 of the Supporting Information (see also Table S2 and Figure S2 for the ΔG_I results). Upon changing the box size, the relative free energies ΔG_I vary over a range of about 4 kJ mol^{-1} at most. These relatively small variations do not indicate that the values are converged to their infinite-size limit (they are almost certainly not) but that the neglected long-range solvation component is of comparable magnitude for all systems. Due to partial error

DOI: 10.1021/acs.jctc.5b00118
J. Chem. Theory Comput. XXXX, XXX, XXX−XXX

Table 4. Comparison between Calculated and Experimental Standard Absolute Binding Free Energies[a]

solvent	Sim./ Exp.		ΔG_I° [kJ mol^{-1}] Li$^+$	Na$^+$	K$^+$	Rb$^+$	Cs$^+$
H_2O	Exp.	12C4	–[d]	–[b]	–[b]	–[b]	–[b]
		15C5	0[c]	−4.6	−4.3	−3.6[d]	−4.6
		18C6	0[c]	−4.6	−12	−8.7	−5.5
H_2O	Sim.	12C4	3.1	−1.3	−3.4	−2.9	−3.8
		15C5	2.6	−3.7	−6.9	−6.5	−7.0
		18C6	−3.1	−11.8	−14.0	−13.2	−11.2
DMSO	Exp.	12C4	0[c]				
		15C5	0[c]	−6.7			
		18C6	0[c]	−8.2	−19		−17
DMSO	Sim.	12C4	−0.1	−14.8	−8.1	−7.9	−8.9
		15C5	−1.1	−16.7	−9.8	−10.0	−12.3
		18C6	−5.1	−29.5	−20.1	−19.6	−19.0
CH_3OH	Exp.	12C4	−7.6	−8.6	−9.2	−9.5	−9.3
		15C5	−7.1	−19	−20	−16	−15
		18C6	0[c]	−25	−35	−31	−26
CH_3OH	Sim.	12C4	−8.9	−14.1	−15.8	−15.1	−14.9
		15C5	−9.7	−13.9	−17.5	−17.8	−17.2
		18C6	−19.7	−33.0	−36.4	−33.5	−30.1

[a]The absolute binding free energies ΔG_I° of eq 9 are reported for the different solvents and hosts (Sim.) considering the simulations in the normal box (L = 3.54 nm), along with the experimental values (Exp.). The experimental values are assumed to pertain to a one molar reference concentration m° = 1 mol dm^{-3}. A dash (−) indicates that complexation was too weak to be monitored. Absent entries indicate the absence of experimental data. Unless otherwise specified (other table footnotes), the experimental data is taken from ref 77. The data is also illustrated graphically in Figure 7. The results including smaller and larger box sizes are reported in Table S3 in the Supporting Information. [b]Reference 71. [c]Reference 69. [d]Reference 70.

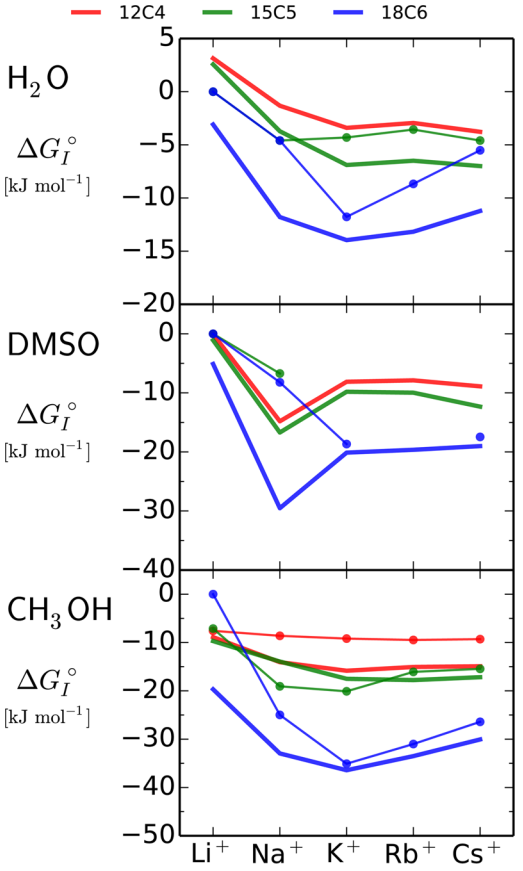

Figure 7. Comparison between calculated and experimental standard absolute binding free energies. The standard absolute binding free energies ΔG_I° of eq 9 are displayed for the different solvents and hosts considering the simulations in the normal box (L = 3.54 nm), and compared to corresponding experimental values. The calculation results are shown using thick lines. The experimental values are shown using thin lines with bullets. This data is also reported numerically in Table 4. The results including smaller and larger box sizes are shown in Figure S3 of the Supporting Information.

cancellation around the thermodynamic cycle, the corresponding variations in the calculated binding free energies ΔG_I° cover a range of about 2 kJ mol^{-1} at most. Comparing the curves corresponding to the three box sizes in Figure S3, these residual finite-size effects appear to still be significant compared to the statistical uncertainties of the calculations, but do not affect the qualitative trends observed along the series of ions for the different systems. Further discussion refers to the simulations performed using a common box size L = 3.54 nm.

Besides possible finite-size errors, the statistical error affecting the MS-λ-LEUS results for ΔG_I° was estimated by performing five independent repeats of the calculations in water (normal box), involving different random-number generator seeds for the initial velocities at the start of the LE-phase. The resulting averages and standard deviations are reported in Table S4 of the Supporting Information. The observed standard deviations suggest a statistical uncertainty on the order of 2 kJ mol^{-1} (2−3 times the standard deviations for a confidence interval of 95−99%) on the ΔG_I° values reported in Table 4. The MS-λ-LEUS results were also compared to those of standard TI calculations for the binding free energies of Li$^+$ and Cs$^+$ to the three hosts in water (normal box). The TI calculations involved 2 × 21 ns equilibration and sampling time for each ΔG_I° value, compared to 2 × 80 ns build-up and sampling time for five ΔG_I° values in MS-λ-LEUS. The resulting TI estimates for ΔG_I° are reported in Table S5 of the Supporting Information. The deviations between the TI and the average MS-λ-LEUS results of Table S4 range between 0 and 3 kJ mol^{-1} (up to 5 kJ mol^{-1} for Li$^+$ with 15C5). This deviation is reasonable considering that the uncertainty affecting the TI results is probably on the same order or higher as that affecting the MS-λ-LEUS results.[47,64]

Considering Table 4 and Figure 7, the agreement between calculation results and experimental data is by no means quantitative, with deviations that typically range between 0 and 6 kJ mol^{-1}, along with a few occurrences (Na$^+$ with 12C4 and 15C5 in DMSO, Li$^+$ with 18C6 in CH_3OH) of much larger discrepancies. These deviations are at least in part related to the approximate nature of the employed force field. In particular, the model employed for the ions[87] has been optimized against hydration free energies, but its use with the present DMSO model[89] or CH_3OH model[90] relies on the application of an empirical (geometric mean) combination rule, and the resulting single-ion solvation properties have never been assessed. The same holds for the compatibility of these parameters with the parameters of the crown ethers in the 53A6$_{OXY+D}$ force field.[85] A compatibility problem of this kind is probably at the source of the anomalously strong (relative to experiment) binding free energy ΔG_I° calculated for Na$^+$ in DMSO, which can be traced back to an unexpectedly low solvation free energy ΔG_I of the ion (relative to Li$^+$ and K$^+$) in this solvent.

DOI: 10.1021/acs.jctc.5b00118
J. Chem. Theory Comput. XXXX, XXX, XXX−XXX

Qualitatively, however, the main experimental trends appear to be captured by the simulations. The trend toward increasingly strong binding for each of the three hosts when going from H_2O to DMSO, and then to CH_3OH, is clearly reproduced. Furthermore, in H_2O and CH_3OH, the positive curvature of the ΔG_I° evolution along the alkali series is also reproduced. In particular, a minimum (most favorable binding) is observed at K^+ for 18C6 in both solvents, in agreement with experiment. The presence of such a curvature and the dependence of the resulting curve on the host size are easily interpreted in terms of two opposite trends affecting the relative free energies ΔG_I in the pure solvent (solvation free energy) and within the host. To facilitate this interpretation, illustrative configurations from the simulations of the different host−guest complexes are displayed in Figure 8.

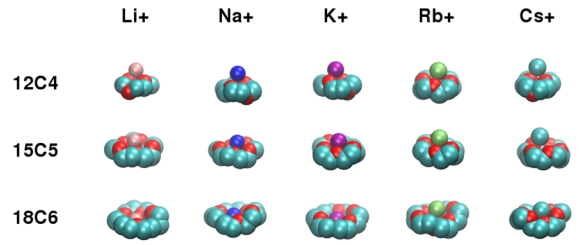

Figure 8. Illustrative configurations of the different host−guest complexes in water. Shown are snapshots taken from the simulations in water for the three different crown ethers and five different cations. The carbon and oxygen atoms of the crown ether are shown in blue and red, respectively.

In accordance with the Born model,[104] the relative free energy ΔG_I of the solvated ion (solvation free energy) decreases in magnitude when the ionic size increases, i.e. along the cation series. However, the direct Coulombic interactions between the ion and the host are expected to become weaker as the ionic size increases, because the ion increasingly protrudes outside the host cavity. This effect is encompassed within the relative free energy ΔG_I of the host−guest complex, although the latter quantity still decreases in magnitude along the cation series because it is dominated by the effect of the solvent surrounding the complex.

For 12C4, the size of the binding cavity is so small that it cannot properly accommodate any ion of the series. As a result, the binding is weak, and the trend along the series is dominated by the dependence of the solvation free energy on the ionic size. For 15C5, the size of the binding cavity is somewhat larger, but the ions still protrude outside this cavity. As a result, although the binding is stronger, the trend along the series is still dominated by that in the solvation free energy. For 18C6, however, the cavity becomes sufficiently large, and the trend along the K^+, Rb^+, and Cs^+ series is now dominated by the dependence of the direct host−guest Coulombic interactions on the ionic size, i.e. ΔG_I° increases now from K^+ to Rb^+ and from Rb^+ to Cs^+. The situation along the Li^+, Na^+, and K^+ series is different because they all fit perfectly within the cavity. Since the distance between the ion and the crown-ether oxygen atoms is essentially fixed, the direct host−guest Coulombic interactions are about the same for the three ions. As a result, the trend for these ions is again dominated by the solvation free energy, i.e. ΔG_I° decreases from Li^+ to Na^+ and from Na^+ to K^+. This results in the minimum observed at K^+ in the ΔG_I° curve for 18C6 and in the selectivity of 18C6 for this specific ion. In other words, when multiple guests fit equally well into the cavity of a relatively rigid host and present direct host−guest interactions of comparable magnitudes, then the least solvated will have the highest binding affinity.

5. CONCLUSIONS

The present article proposed an extension of the λ-LEUS scheme[47] to the MS situation, enabling the calculation of the relative free energies of multiple physical states based on a single simulation.

Compared to the other available MS schemes, namely OSP,[28−30] EDS,[35] and λD,[37−41] the MS-λ-LEUS scheme presents a number of key advantages, namely: (*i*) the physical states are visited explicitly and over finite time periods, rather than being reached by extrapolation (reweighting) or visited during infinitesimal times (as in λD); (*ii*) the extent of unphysical space required to ensure transitions is kept minimal and, in particular, one-dimensional; (*iii*) the setup protocol solely requires the topologies of the physical states, rather than relying on a carefully designed unphysical (e.g., soft-core or EDS-combined) reference state; and (*iv*) the method only requires limited modifications in an MD simulation code that is able to handle two-state mutations.

The MS scheme presented in this article was applied together with the λD variant[47,63] of the LEUS method,[48] but it could as well be implemented within a well-tempered metadynamics[111] (WTM) scheme. The finite-temperature interval[111] ΔT in WTM plays a similar role as the force-reduction mechanism[19,47] during the LE-phase of LEUS. Both lead to a progressive reduction of the build-up rate in time, thereby ensuring the convergence of the biasing potential in the infinite-time limit. The main difference between the two approaches is that in WTM, the entire simulation time is invested into the build-up phase with a time-dependent Hamiltonian, and the free-energy profile is estimated indirectly as the negative of the final biasing potential. In contrast, in LEUS, only part of the simulation time is invested into the analogous LE-phase. The rest is kept for the subsequent US-phase, and the free-energy profile is estimated directly by reweighting the configurational probability distribution obtained from the equilibrium sampling with a time-independent Hamiltonian. One may argue that, owing to this true equilibrium sampling, LEUS provides a more accurate free-energy estimate. However, the WTM scheme leads to an estimate that relies on the entire simulation time whereas in LEUS, the sampling statistics of the LE-phase is discarded. At present, the relative efficiency-to-accuracy ratios of the two methods are unknown, and they may actually depend heavily on the parameters employed in the two methods and on the problem considered (e.g., dimensionality and ruggedness of the free-energy energy surface).

As noted in previous work,[47,63,64] schemes relying on a dynamical evolution of the alchemical variable offer an enhanced sampling ability (relative to TI) in the orthogonal space, an advantage shared with Hamiltonian replica-exchange (HR) procedures.[112,113] Here, the term orthogonal[62,114,115] refers to all the degrees of freedom that are not subjected to the primary sampling enhancement. In the case of an alchemical free-energy calculation, the primary sampling enhancement (e.g., TI, HR or λ-LEUS) affects λ only, and the orthogonal space is defined by all the physical degrees of freedom of the system. When λ is constrained in separate simulations (TI), barriers in the orthogonal space (slow conformational

DOI: 10.1021/acs.jctc.5b00118
J. Chem. Theory Comput. XXXX, XXX, XXX−XXX

relaxation processes) may hinder the sampling at each λ point.[73,116] In contrast, when λ is allowed to change in a discrete (HR) or continuous (λ-LEUS) fashion during the simulation, λ-dependent pathways may open up to circumvent these barriers. Pictorially, the crossing between two different valleys on the potential-energy surface in the orthogonal space may be very difficult at a specific λ-value where they are separated by a high mountain range, but become easy if the transition can occur via another λ-value where the valleys are connected by a low pass or even converge. In some situations, however, this advantage may not be sufficient, and one may rely on an additional sampling-enhancement technique targeting specifically the orthogonal space. Such combinations involving both primary (along the degrees of freedom defining the PMF to be calculated) and secondary (along the orthogonal ones) sampling enhancements have proved remarkably efficient and involve secondary enhancements by, e.g.: (*i*) random walking;[114,117] (*ii*) tempering[62,115] or parallel tempering;[118] (*iii*) potential-energy scaling,[119] smoothing[120,121] (e.g., soft-core), or biasing[122,123] (e.g., using US); and (*iv*) restraining or confinement.[19,42,124,125] It may also be of interest to reconsider the functional form of the alchemical coupling between the physical states,[100−128] so as to design more advanced schemes that automatically restrict the size of the accessible orthogonal space and simplify its features along the λ-pathway[124,129−131] (low-variance pathways). In principle, these two types of approaches (secondary sampling enhancement and improved coupling schemes) can easily be combined with MS-λ-LEUS. An additional possible extension of MS-λ-LEUS would be the connection of the physical states by a redundant tree of paths[19,132] rather than by a single cyclic one, trying to gain further efficiency in the spirit of the replica-permutation (nonpairwise) HR implementations of refs 133−135. Another extension would be the development of a twin-system[136] variant of MS-λ-LEUS, where the mutations within the host and free in solution would be performed concurrently in opposite directions. The latter setup would permit the calculation of multiple binding free energies from a single simulation, rather than from a simulation pair, with a potential efficiency gain arising from the partial cancellation of the driving forces in the two environments.

As an initial application, the calculation of the absolute binding free energies of five alkali cations to three crown-ether hosts considering three different solvents was reported. For each solvent and environment (bound to a given host or free in solution), the calculation of the relative free energies of the five ions (plus the dummy state) required a single MS-λ-LEUS calculation. The results were found to reproduce qualitatively the main experimental trends. In particular, tendentially stronger binding was observed along the solvent series from H_2O to DMSO, and then to CH_3OH. Of special interest is the reproduction of the experimental selectivity of 18C6 for K^+ in H_2O and CH_3OH (minimum in the binding free energy along the cation series). This selectivity results from opposing trends in the solvation free energy of the cation and in the direct electrostatic interactions within the complex along the ion series. The ions Li^+, Na^+, and K^+ bind increasingly well to 18C6 because they fit into the host cavity with comparable direct interactions, and are decreasingly well solvated. In contrast, the ions K^+, Rb^+, and Cs^+ bind decreasingly strongly because they protrude outside the host cavity, and the decreasing strength of these direct interactions dominates over the decreasing strength of their solvation. Interestingly, a similar phenomenon is probably at the origin of the selectivity of the potassium channel for the K^+ ion over the Na^+ ion.[137]

Of course, this initial application of the MS-λ-LEUS scheme is relatively nonchallenging in terms of the selected perturbation, which involves the mutation of a single atom, a predominantly linear environment response (charge change), and relatively fast orthogonal relaxation processes (solvent and ether responses). However, the feasibility of the two-state λ-LEUS scheme has already been assessed in a more complex situation,[64] and work is in progress to apply the newly developed MS variant to challenging problems, in particular in the context of protein−ligand binding with an eye on drug-design applications.

■ ASSOCIATED CONTENT

Supporting Information

Results from additional simulations with different box sizes and additional simulations for error estimation. The Supporting Information is available free of charge on the ACS Publications website at DOI: 10.1021/acs.jctc.5b00118.

■ AUTHOR INFORMATION

Corresponding Author

*Phone: 41 44 632 55 03. Fax: 41 44 632 10 39. E-mail: phil@igc.phys.chem.ethz.ch.

Notes

The authors declare no competing financial interest.

■ ACKNOWLEDGMENTS

Financial support from the Swiss National Science Foundation (Grants 21-132739 and 21-138020) is gratefully acknowledged.

■ REFERENCES

(1) Steed, J. W.; Atwood, J. L. In *Supramolecular Chemistry*, 2nd ed.; John Wiley & Sons: Chichester, UK, 2009.

(2) Kern, D.; Zuiderweg, E. R. P. The role of dynamics in allosteric regulation. *Curr. Opin. Struct. Biol.* **2003**, *13*, 748.

(3) McGeagh, J. D.; Ranaghan, K. E.; Mulholland, A. J. Protein dynamics and enzyme catalysis: Insights from simulations Biochim. *Biophys. Acta* **2011**, *1814*, 1077.

(4) Somorjai, G. A.; Li, Y. In *Introduction to surface chemistry and catalysis*; John Wiley & Sons: Hoboken, NJ, 2010.

(5) Bohacek, R. S.; McMartin, C.; Guida, W. C. The art and practice of structure-based drug design: A molecular moldeing perspective. *Med. Res. Rev.* **1996**, *16*, 3.

(6) Bodor, N.; Buchwald, P. Soft drug design: General principles and recent applications. *Med. Res. Rev.* **2000**, *20*, 58.

(7) van Gunsteren, W. F.; Berendsen, H. J. C. Computer simulation of molecular dynamics: Methodology, applications and perspectives in chemistry. *Angew. Chem., Int. Ed.* **1990**, *29*, 992.

(8) van Gunsteren, W. F.; Bakowies, D.; Baron, R.; Chandrasekhar, I.; Christen, M.; Daura, X.; Gee, P.; Geerke, D. P.; Glättli, A.; Hünenberger, P. H.; Kastenholz, M. A.; Oostenbrink, C.; Schenk, M.; Trzesniak, D.; van der Vegt, N. F. A.; Yu, H. B. Biomolecular modelling: goals, problems, perspectives. *Angew. Chem., Int. Ed.* **2006**, *45*, 4064.

(9) Christ, C. D.; Mark, A. E.; van Gunsteren, W. F. Basic ingredients of free energy calculations: A review. *J. Comput. Chem.* **2010**, *31*, 1569.

(10) Hansen, N.; van Gunsteren, W. F. Practical aspects of free-energy calculations: a review. *J. Chem. Theory Comput.* **2014**, *10*, 2632.

(11) Mobley, D. L.; Klimovich, P. V. Perspective: Alchemical free energy calculations for drug discovery. *J. Chem. Phys.* **2012**, *137*, 230901/1.

DOI: 10.1021/acs.jctc.5b00118
J. Chem. Theory Comput. XXXX, XXX, XXX−XXX

(12) Christ, C. D.; Fox, T. Accuracy assessment and automation of free energy calculations for drug design. *J. Chem. Inf. Model.* **2014**, *54*, 108.
(13) Best, R. B.; Buchete, N.-V.; Hummer, G. Are current molecular dynamics force fields too helical? *Biophys. J.* **2008**, *95*, L07.
(14) Lindorff-Larse, K.; Maragakis, P.; Piana, S.; Eastwood, M. P.; Dror, R. O.; Shaw, D. E. Systematic validation of protein force fields against experimental data. *PLoS One* **2012**, *7*, e32131.
(15) Piggot, T. J.; Piñeiro, A.; Khalid, S. Molecular dynamics simulations of phosphatidylcholine membranes: A comparative force field study. *J. Chem. Theory Comput.* **2012**, *8*, 4593.
(16) Cino, E. A.; Choy, W.; Karttunen, M. Comparison of secondary structure formation using 10 different force fields in microsecond molecular dynamics simulations. *J. Chem. Theory Comput.* **2012**, *8*, 2725.
(17) Christen, M.; van Gunsteren, W. F. On searching in, sampling of, and dynamically moving through conformational space of biomolecular systems: A review. *J. Comput. Chem.* **2008**, *29*, 157.
(18) Hansen, H. S.; Daura, X.; Hünenberger, P. H. Enhanced conformational sampling in molecular dynamics simulations of solvated peptides: fragment-based local elevation umbrella sampling. *J. Chem. Theory Comput.* **2010**, *6*, 2598.
(19) Hansen, H. S.; Hünenberger, P. H. Ball-and-stick local elevation umbrella sampling: molecular simulations involving enhanced sampling within conformational or alchemical subspaces of low internal dimensionalities, minimal irrelevant volume and problem-adapted geometries. *J. Chem. Theory Comput.* **2010**, *6*, 2622.
(20) Bruckner, S.; Boresch, S. Efficiency of alchemical free energy simulations. I. A practical comparison of the exponential formula, thermodynamic integration, and Bennett's acceptance ratio method. *J. Comput. Chem.* **2011**, *32*, 1303.
(21) Bruckner, S.; Boresch, S. Efficiency of alchemical free energy simulations. II. Improvements for thermodynamic integration. *J. Comput. Chem.* **2011**, *32*, 1320.
(22) Hünenberger, P. H.; Granwehr, J. K.; Aebischer, J.-N.; Ghoneim, N.; Haselbach, E.; van Gunsteren, W. F. Experimental and theoretical approaches to hydrogen-bonded diastereomeric interactions in a model complex. *J. Am. Chem. Soc.* **1997**, *119*, 7533.
(23) Ghoufi, A.; Malfreyt, P. Calculations of the absolute thermodynamic properties of association of host-guest systems from the intermolecular potential of mean force. *J. Chem. Phys.* **2006**, *125*, 224503/1.
(24) de Ruiter, A.; Oostenbrink, C. Protein-ligand binding from distancefield distances and Hamiltonian replica exchange simulations. *J. Chem. Theory Comput.* **2013**, *9*, 883.
(25) Zeller, F.; Zacharias, M. Adaptive biasing combined with Hamiltonian replica exchange to improve umbrella sampling free energy simulations. *J. Chem. Theory Comput.* **2014**, *10*, 703.
(26) Jorgensen, W. L.; Buckner, J. K.; Boudon, S.; Tirado-Rives, J. Efficient computation of absolute free energies of binding by computer simulations. Application to the methane dimer in water. *J. Chem. Phys.* **1988**, *89*, 3742.
(27) Gilson, M. K.; Given, J. A.; Bush, B. L.; McCammon, J. A. The statistical thermodynamic basis for computation of binding-affinities. A critical review. *Biophys. J.* **1997**, *72*, 1047.
(28) Mark, A. E.; Xu, Y.; Liu, H.; van Gunsteren, W. F. Rapid non-empirical approaches for estimating relative binding free energies. *Acta Biochim. Polym.* **1995**, *42*, 525.
(29) Liu, H.; Mark, A. E.; van Gunsteren, W. F. Estimating the relative free energy of different molecular states with respect to a single reference state. *J. Phys. Chem.* **1996**, *100*, 9485.
(30) Pitera, J. W.; van Gunsteren, W. F. One-step perturbation methods for solvation free energies of polar solutes. *J. Phys. Chem. B* **2001**, *105*, 11264.
(31) Khavrutskii, I. V.; Wallqvist, A. Computing relative free energies of solvation using single reference thermodynamic integration augmented with Hamiltonian replica exchange. *J. Chem. Theory Comput.* **2010**, *6*, 3427.
(32) Khavrutskii, I. V.; Wallqvist, A. Improved binding free energy predictions from single-reference thermodynamic integration augmented with Hamiltonian replica exchange. *J. Chem. Theory Comput.* **2011**, *7*, 3001.
(33) Oostenbrink, C.; van Gunsteren, W. F. Free energies of binding of polychlorinated biphenyls to the estrogen receptor from a single simulation. *Proteins: Struct., Funct., Genet.* **2004**, *54*, 234.
(34) Hritz, J.; Oostenbrink, C. Efficient free energy calculations for compounds with multiple stable conformations separated by high energy barriers. *J. Phys. Chem. B* **2009**, *113*, 12711.
(35) Christ, C. D.; van Gunsteren, W. F. Multiple free energies from a single simulation: Extending enveloping distribution sampling to nonoverlapping phase-space distributions. *J. Chem. Phys.* **2008**, *128*, 174112/1.
(36) Kong, X.; Brooks, C. L., III λ-dynamics: A new approach to free energy calculations. *J. Chem. Phys.* **1996**, *105*, 2414.
(37) Guo, Z.; Brooks, C. L., III; Kong, X. Efficient and flexible algorithm for free energy calculations using the λ-dynamics approach. *J. Phys. Chem. B* **1998**, *102*, 2032.
(38) Khandogin, J.; Brooks, C. L. Constant pH molecular dynamics with proton tautomerism. *Biophys. J.* **2005**, *89*, 141.
(39) Knight, J. L.; Brooks, C. L., III λ-dynamics free energy simulation methods. *J. Comput. Chem.* **2009**, *30*, 1692.
(40) Knight, J. L.; Brooks, C. L., III Multisite λ-dynamics for simulated structure-activity relationship studies. *J. Chem. Theory Comput.* **2011**, *7*, 2728.
(41) Armacost, K. A.; Goh, G. B.; Brooks, C. L., III Biasing potential replica exchange multisite dynamics for efficient free energy calculations. *J. Chem. Theory Comput.* **2015**, *11*, 1267.
(42) Bieler, N. S.; Hünenberger, P. H. On the ambiguity of conformational states: a B&S-LEUS simulation study of the helical conformations of decaalanine in water. *J. Chem. Phys.* **2015**, *142*, 165102/1.
(43) Oostenbrink, C.; van Gunsteren, W. F. Single-step perturbations to calculate free energy differences from unphysical reference states: limits on size, flexibility and character. *J. Comput. Chem.* **2003**, *24*, 1730.
(44) Lin, Z.; van Gunsteren, W. F. The effect of branched side chains on the relative stability of α- and π-helices: a combination of the enveloping distribution sampling and one-step perturbation methods. *Mol. Phys.* **2013**, *111*, 2126.
(45) Lin, Z.; van Gunsteren, W. F. On the choice of a reference state for one-step perturbation calculations between polar and nonpolar molecules in polar environments. *J. Comput. Chem.* **2013**, *34*, 387.
(46) Smith, P. E.; van Gunsteren, W. F. Predictions of free energy differences from a single simulation of the initial state. *J. Chem. Phys.* **1994**, *100*, 577.
(47) Bieler, N. S.; Häuselmann, R.; Hünenberger, P. H. Local elevation umbrella sampling applied to the calculation of alchemical free-energy changes via λ-dynamics: The λ-LEUS scheme. *J. Chem. Theory Comput.* **2014**, *10*, 3006.
(48) Hansen, H. S.; Hünenberger, P. H. Using the local elevation method to construct optimized umbrella sampling potentials: Calculation of the relative free energies and interconversion barriers of glucopyranose ring conformers in water. *J. Comput. Chem.* **2010**, *31*, 1.
(49) Huber, T.; Torda, A. E.; van Gunsteren, W. F. Local elevation: A method for improving the searching properties of molecular dynamics simulation. *J. Comput.-Aided Mol. Des.* **1994**, *8*, 695.
(50) Torrie, G. M.; Valleau, J. P. Nonphysical sampling distributions in Monte Carlo free-energy estimation: Umbrella sampling. *J. Comput. Phys.* **1977**, *23*, 187.
(51) Kirkwood, J. G. Quantum statistics of almost classical assemblies. *Phys. Rev.* **1933**, *44*, 31.
(52) Kirkwood, J. G. Quantum statistics of almost classical assemblies. *Phys. Rev.* **1934**, *45*, 116.
(53) Kirkwood, J. G. Statistical mechanics of fluid mixtures. *J. Chem. Phys.* **1935**, *3*, 300.

DOI: 10.1021/acs.jctc.5b00118
J. Chem. Theory Comput. XXXX, XXX, XXX−XXX

(54) Zwanzig, R. W. High-temperature equation of state by a perturbation method. I. Nonpolar gases. *J. Chem. Phys.* **1954**, *22*, 1420.
(55) Tidor, B. Simulated annealing on free energy surfaces by a combined molecular dynamics and Monte Carlo approach. *J. Phys. Chem.* **1993**, *97*, 1069.
(56) Jarzynski, C. Nonequilibrium equality for free energy differences. *Phys. Rev. Lett.* **1997**, *78*, 2690.
(57) Jarzynski, C. Equilibrium free-energy differences from nonequilibrium measurements: A master-equation approach. *Phys. Rev. E* **1997**, *56*, 5018.
(58) Knight, J. L.; Brooks, C. L., III Applying efficient implicit nongeometric constraints in alchemical free energy simulations. *J. Comput. Chem.* **2011**, *32*, 3423.
(59) Donnini, S.; Tegeler, F.; Groenhof, G.; Grubmüller, H. Constant pH molecular dynamics in explicit solvent with λ-dynamics. *J. Chem. Theory Comput.* **2011**, *7*, 1962.
(60) Donnini, S.; Tegeler, F.; Groenhof, G.; Grubmüller, H. Correction to constant pH molecular dynamics in explicit solvent with λ-dynamics. *J. Chem. Theory Comput.* **2013**, *9*, 3261.
(61) Wu, P.; Hu, X.; Yang, W. λ-metadynamics approach to compute absolute solvation free energy. *J. Phys. Chem. Lett.* **2011**, *2*, 2099.
(62) Zheng, L.; Yang, W. Practically efficient and robust free energy calculations: Double-integration orthogonal space tempering. *J. Chem. Theory Comput.* **2012**, *8*, 810.
(63) Bieler, N. S.; Hünenberger, P. H. Communication: Estimating the initial biasing potential for λ-local-elevation umbrella-sampling (λ-LEUS) simulations via slow growth. *J. Chem. Phys.* **2014**, *141*, 201101.
(64) Bieler, N. S.; Hünenberger, P. H. Orthogonal sampling in free-energy calculations of residue mutations in a tripeptide: TI vs. λ-LEUS. *J. Comput. Chem.* **2015**, submitted.
(65) Pedersen, C. J. Cyclic polyether and their complexes with metal salts. *J. Am. Chem. Soc.* **1967**, *89*, 7017.
(66) Gokel, G. W.; Goli, D. M.; Minganti, C.; Echegoyen, L. Clarification of the hole-size cation-diameter relationship in crown ethers and a new method for determining calcium cation homogeneous equilibrium binding constants. *J. Am. Chem. Soc.* **1983**.
(67) Beresford, G. D.; Stoddart, J. F. The synthesis and complexing properties of oxo-12-crown-3 and 18-crown-5. *Tetrahedron Lett.* **1980**, *21*, 867.
(68) Lamb, J. D.; Izatt, R. M.; Swain, C. S.; Christensen, J. J. A systematic study of the effect macrocyle ring size and donor atom type on the log K, ΔH, and TΔS of reactions at 25degrC in methanol of mono- and divalent cations with crown ethers. *J. Am. Chem. Soc.* **1980**, *102*, 475−479.
(69) Smetana, A. J.; Popov, A. I. Lithium-7 nuclear magnetic resonance and calorimetric study of lithium crown complexes in various solvents. *J. Sol. Chem.* **1980**, *8*, 183.
(70) Izatt, R. M.; Terry, R. E.; Haymore, B. L.; Hansen, L. D.; Dalley, N. K.; Ayondet, A. G.; Christensen, J. J. Calorimetric titration study of the interaction of several uni- and bivalent cations with 15-crown-5, 18-crown-6, and two isomers of dicyclohexo-18-crown-6 in aqueous solution at 25°C and μ = 0.1. *Chem. Rev.* **1976**, *85*, 271.
(71) Hoiland, H.; Ringseth, J. A.; Brun, T. S. Cation-crown ether complex formation in water. II. Alkali and alkaline earth cations and 12-crown-4, 15-crown-5, and 18-crown-6. *J. Sol. Chem.* **1979**, *8*, 779−792.
(72) Thompson, M. A.; Glendening, E. D.; Feller, D. The nature of K^+/crown ether interactions: A hybrid quantum mechanical-molecular mechanical study. *J. Phys. Chem.* **1994**, *98*, 10465.
(73) Straatsma, T. P.; McCammon, J. A. Treatment of rotational isomers in free energy calculations. II. Molecular dynamics simulation study of 18-crown-6 in aqueous solution as an example of systems with large numbers of rotational isomeric states. *J. Chem. Phys.* **1989**, *91*, 3631.
(74) Dang, L. X.; Kollman, P. A. Free energy of association of the K^+:18-crown-6 complex in water: A new molecular dynamics study. *J. Phys. Chem.* **1995**, *99*, 55.
(75) Dang, L. X. Mechanism and thermodynamics of ion selectivity in aqueous solutions of 18-crown-6 ether: A molecular-dynamics study. *J. Am. Chem. Soc.* **1995**, *117*, 6954.
(76) Martínez-Haya, B.; Hurtado, P.; Hortal, A. R.; Hamad, S.; Steill, J. D.; Oomens, J. Emergence of symmetry and chirality in crown ether complexes with alkali metal cations. *J. Phys. Chem. A* **2010**, *114*, 7048.
(77) Arnaud-Neu, F.; Delgado, R.; Chaves, S. Critical evaluation of stability constants and thermodynamic functions of metal complexes of crown ethers. *Pure Appl. Chem.* **2003**, *75*, 71.
(78) Boresch, S.; Tettinger, F.; Leitgeb, M.; Karplus, M. Absolute binding free energies: A quantitative approach for their calculation. *J. Phys. Chem. B* **2003**, *107*, 9535.
(79) Deng, Y.; Roux, B. Calculation of standard binding free energies: Aromatic molecules in the T4 lysozyme L99A mutant. *J. Chem. Theory Comput.* **2006**, *2*, 1255.
(80) Rocklin, G. J.; Mobley, D. L.; Dill, K. A.; Hünenberger, P. H. Calculating the binding free energies of charged species based on explicit-solvent simulations employing lattice-sum methods: An accurate correction scheme for electrostatic finite-size effects. *J. Chem. Phys.* **2013**, *139*, 184103/1.
(81) Reif, M. M.; Oostenbrink, C. Net charge changes in the calculation of relative ligand-binding free energies *via* classical atomistic molecular dynamics simulations. *J. Comput. Chem.* **2014**, *35*, 227.
(82) Schmid, N.; Christ, C. D.; Christen, M.; Eichenberger, A. P.; van Gunsteren, W. F. Architecture, implementation and parallelisation of the GROMOS software for biomolecular simulation. *Comput. Phys. Commun.* **2012**, *183*, 890.
(83) Kunz, A.-P. E.; Allison, J. R.; Geerke, D. P.; Horta, B. A. C.; Hünenberger, P. H.; Riniker, S.; Schmid, N.; van Gunsteren, W. F. New functionalities in the GROMOS biomolecular simulation software. *J. Comput. Chem.* **2012**, *33*, 340.
(84) van Gunsteren, W. F. *The GROMOS software for biomolecular simulation*. 2011. http://www.gromos.net (accessed 05/05/2011).
(85) Fuchs, P. F. J.; Hansen, H. S.; Hünenberger, P. H.; Horta, B. A. C. A GROMOS parameter set for vicinal diether functions: properties polyethyleneoxide and polyethyleneglycol. *J. Chem. Theory Comput.* **2012**, *8*, 3943.
(86) Horta, B. A. C.; Fuchs, P. F. J.; van Gunsteren, W. F.; Hünenberger, P. H. New interaction parameters for oxygen compounds in the GROMOS force field: Improved pure-liquid and solvation properties for alcohols, ethers, aldehydes, ketones, carboxylic acids and esters. *J. Chem. Theory Comput.* **2011**, *7*, 1016.
(87) Reif, M. M.; Hünenberger, P. H. Computation of methodology-independent single-ion solvation properties from molecular simulations. IV. Optimized Lennard-Jones parameter sets for the alkali and halide ions in water. *J. Chem. Phys.* **2011**, *134*, 144104/1.
(88) Berendsen, H. J. C.; Postma, J. P. M.; van Gunsteren, W. F.; Hermans, J. In *Intermolecular Forces*; Pullman, B., Ed.; Reidel, Dordrecht: The Netherlands, 1981; pp 331−342.
(89) Geerke, D. P.; Oostenbrink, C.; van der Vegt, N. F. A.; van Gunsteren, W. F. An effective force field for molecular dynamics simulations of dimethyl sulfoxide and dimethyl sulfoxide-water mixtures. *J. Phys. Chem. B* **2004**, *108*, 1436.
(90) Walser, R.; Mark, A. E.; van Gunsteren, W. F.; Lauterbach, M.; Wipff, G. The effect of force-field parameters on properties of liquids: Parametrization of a simple three-site model for methanol. *J. Chem. Phys.* **2000**, *112*, 10450.
(91) Hockney, R. W. The potential calculation and some applications. *Methods Comput. Phys.* **1970**, *9*, 135.
(92) Ryckaert, J.-P.; Ciccotti, G.; Berendsen, H. J. C. Numerical integration of the Cartesian equations of motion of a system with constraints: Molecular dynamics of *n*-alkanes. *J. Comput. Phys.* **1977**, *23*, 327.
(93) Berendsen, H. J. C.; Postma, J. P. M.; van Gunsteren, W. F.; di Nola, A.; Haak, J. R. Molecular dynamics with coupling to an external bath. *J. Chem. Phys.* **1984**, *81*, 3684.
(94) Lide, D. R. In *CRC Handbook of Chemistry and Physics*, 80th ed.; CRC Press: Boca Raton, FL, 1999.

DOI: 10.1021/acs.jctc.5b00118
J. Chem. Theory Comput. XXXX, XXX, XXX−XXX

(95) Rigby, M.; Smith, E. B.; Wakeham, W. A.; Maitland, G. C. In *The forces between molecules*; Clarendon Press: Oxford, UK, 1986.
(96) Berendsen, H. J. C.; van Gunsteren, W. F.; Zwinderman, H. R. J.; Geurtsen, R. G. Simulations of proteins in water. *Ann. N. Y. Acad. Sci.* **1986**, *482*, 269.
(97) Barker, J. A.; Watts, R. O. Monte Carlo studies of the dielectric properties of water-like models. *Mol. Phys.* **1973**, *26*, 789.
(98) Tironi, I. G.; Sperb, R.; Smith, P. E.; van Gunsteren, W. F. A generalized reaction field method for molecular dynamics simulations. *J. Chem. Phys.* **1995**, *102*, 5451.
(99) Heinz, T. N.; van Gunsteren, W. F.; Hünenberger, P. H. Comparison of four methods to compute the dielectric permittivity of liquids from molecular dynamics simulations. *J. Chem. Phys.* **2001**, *115*, 1125.
(100) Beutler, T. C.; Mark, A. E.; van Schaik, R.; Gerber, P. R.; van Gunsteren, W. F. Avoiding singularities and numerical instabilities in free energy calculations based on molecular simulations. *Chem. Phys. Lett.* **1994**, *222*, 529.
(101) Habermann, C.; Kindermann, F. Multidimensional spline interpolation: Theory and applications. *Comput. Econ.* **2007**, *30*, 153.
(102) Babin, V.; Roland, C.; Sagui, C. Adaptively biased molecular dynamics for free energy calculations. *J. Chem. Phys.* **2008**, *128*, 134101/1.
(103) Martyna, G. J.; Klein, M. L.; Tuckerman, M. Nosé-Hoover chains: The canonical ensemble via continuous dynamics. *J. Chem. Phys.* **1992**, *97*, 2635.
(104) Born, M. Volumen und Hydrationswärme der Ionen. *Z. Phys.* **1920**, *1*, 45.
(105) Hünenberger, P. H.; Reif, M. M. *In Single-ion solvation: Experimental and theoretical approaches to elusive thermodynamic quantities*, 1st ed.; Royal Society of Chemistry: London, UK, 2011 (Theoretical and Computational Chemistry Series).
(106) Kelly, C. P.; Cramer, C. J.; Truhlar, D. G. Single-ion solvation free energies and the normal hydrogen electrode potential in methanol, acetonitrile, and dimethyl sulfoxide. *J. Phys. Chem. B* **2007**, *111*, 408.
(107) Swain, C. G.; Swain, M. S.; Powell, A. L.; Alunni, S. Solvent effects on chemical reactivity. Evaluation of anion- and cation-solvation components. *J. Am. Chem. Soc.* **1983**, *105*, 502.
(108) Bardhan, J. P.; Jungwirth, P.; Makowski, L. Affine-response model of molecular solvation of ions: Accurate predictions of asymmetric charging free energies. *J. Chem. Phys.* **2012**, *137*, 124101/1.
(109) Kastenholz, M. A.; Hünenberger, P. H. Computation of methodology-independent ionic solvation free energies from molecular simulations. II. The hydration free energy of the sodium cation. *J. Chem. Phys.* **2006**, *124*, 224501/1.
(110) Reif, M. M.; Hünenberger, P. H. Computation of methodology-independent single-ion solvation properties from molecular simulations. III. Correction terms for the solvation free energies, enthalpies, entropies, heat capacities, volumes, compressibilities and expansivities of solvated ions. *J. Chem. Phys.* **2011**, *134*, 144103/1.
(111) Barducci, A.; Bussi, G.; Parrinello, M. Well-tempered metadynamics: A smoothly converging and tunable free-energy method. *Phys. Rev. Lett.* **2008**, *100*, 020603/1.
(112) Sugita, Y.; Okamoto, Y. Replica-exchange molecular dynamics method for protein folding. *Chem. Phys. Lett.* **1999**, *134*, 141.
(113) Fukunishi, H.; Watanabe, O.; Takada, S. On the Hamiltonian replica exchange method for efficient sampling of biomolecular systems: Application to protein structure prediction. *J. Chem. Phys.* **2002**, *116*, 9058.
(114) Zheng, L.; Chen, M.; Yang, W. Random walk in orthogonal space to achieve efficient free-energy simulation of complex systems. *Proc. Natl. Acad. Sci. U. S. A.* **2008**, *105*, 20227.
(115) Yang, M.; Yang, L.; Gao, Y.; Hu, H. Combine umbrella sampling with integrated tempering method for efficient calculation of free energy changes of complex energy surface. *J. Chem. Phys.* **2014**, *141*, 044108/1.
(116) Straatsma, T. P.; McCammon, J. A. Treatment of rotational isomers in free energy evaluations. Analysis of the evaluation of free energy differences by molecular dynamics simulations of systems with rotational isomeric states. *J. Chem. Phys.* **1989**, *90*, 3300.
(117) Zheng, L.; Chen, M.; Yang, W. Simultaneous escaping of explicit and hidden free energy barriers: Application of the orthogonal space random walk strategy in generalized ensemble based conformational sampling. *J. Chem. Phys.* **2009**, *130*, 234105/1.
(118) Bussi, G.; Gervasio, F. L.; Laio, A.; Parrinello, N. Free-energy landscape for β-haripin folding from combined parallel tempering and metadynamics. *J. Am. Chem. Soc.* **2006**, *128*, 13435.
(119) Kaus, J. W.; Arrar, M.; McCammon, J. A. Accelerated adaptive integration method. *J. Phys. Chem. B* **2014**, *118*, 5109.
(120) Hritz, J.; Oostenbrink, C. Optimization of replica exchange molecular dynamics by fast mimicking interactions. *J. Chem. Phys.* **2007**, *127*, 204104/1.
(121) Hritz, J.; Oostenbrink, C. Hamiltonian replica exchange molecular dynamics using soft-core interactions. *J. Chem. Phys.* **2008**, *128*, 144121/1.
(122) Leitgeb, M.; Schröder, C.; Boresch, S. Alchemical free energy calculations and multiple conformational substates. *J. Chem. Phys.* **2005**, *122*, 084109/1.
(123) Garate, J. A.; Oostenbrink, C. Free energy differences between states with different conformational ensembles. *J. Comput. Chem.* **2013**, *34*, 1398.
(124) Christen, M.; Kunz, A.-P. E.; van Gunsteren, W. F. Sampling of rare events using hidden restraints. *J. Phys. Chem. B* **2006**, *110*, 8488.
(125) Mobley, D. L.; Chodera, J. D.; Dill, K. A. Confine-and-release method: Obtaining correct binding free energies in the presence of protein conformational change. *J. Chem. Theory Comput.* **2007**, *3*, 1231.
(126) Dejaegere, A.; Karplus, M. Analysis of coupling schemes in free energy simulations: A unified description of nonbonded contributions to solvation free energies. *J. Phys. Chem.* **1996**, *100*, 11148.
(127) Buelens, F. P.; Grubmüller, H. Linear-scaling soft-core scheme for alchemical free energy calculations. *J. Comput. Chem.* **2012**, *33*, 25.
(128) Steinbrecher, T.; Mobley, D. L.; Case, D. A. Nonlinear scaling schemes for Lennard-Jones interactions in free energy calculations. *J. Chem. Phys.* **2007**, *127*, 214108/1.
(129) Blondel, A. Ensemble variance in free energy calculations by thermodynamic integration: theory, optimal "alchemical" path, and practical solutions. *J. Comput. Chem.* **2004**, *25*, 985.
(130) Pham, T. T.; Shirts, M. R. Identifying low variance pathways for free energy calculations of molecular transformations in solution phase. *J. Chem. Phys.* **2011**, *135*, 034114/1.
(131) Naden, L. N.; Pham, T. T.; Shirts, M. R. Linear basis function approach to efficient alchemical free energy calculations. 1. Removal of uncharged atomic sites. *J. Chem. Theory Comput.* **2014**, *10*, 1128.
(132) Krause, E. F. In *Taxicab Geometry*; Dover Publications: New York, USA, 1986.
(133) Chodera, J. D.; Shirts, M. R. Replica exchange and expanded ensemble simulations as Gibbs sampling: Simple improvements for enhanced mixing. *J. Chem. Phys.* **2011**, *135*, 194110/1.
(134) Itoh, S. G.; Okumura, H. Replica-permutation method with the Suwa-Todo algorithm beyond the replica-exchange method. *J. Chem. Theory Comput.* **2013**, *9*, 570.
(135) Itoh, S. G.; Okumura, H. Hamiltonian replica-permutation method and its applications to an alanine dipeptide and amyloid-β(29-42) peptides. *J. Comput. Chem.* **2013**, *34*, 2493.
(136) Hansen, N.; Hünenberger, P. H.; van Gunsteren, W. F. Efficient combination of environment change and alchemical perturbation within the enveloping distribution sampling (EDS) scheme: Twin-system EDS and application to the determination of octanol-water partition coefficients. *J. Chem. Theory Comput.* **2013**, *9*, 1334.
(137) Roux, B. Ion conduction and selectivity in K. channels. *Annu. Rev. Biomol. Struct.* **2005**, *34*, 153.

DOI: 10.1021/acs.jctc.5b00118
J. Chem. Theory Comput. XXXX, XXX, XXX−XXX